

# Driven-dissipative turbulence in exciton-polariton quantum fluids

R. Ferrini<sup>1</sup> and S.V. Koniakhin<sup>1,2</sup>

<sup>1</sup>*Center for Theoretical Physics of Complex Systems,  
Institute for Basic Science (IBS), Daejeon 34126, Republic of Korea*

<sup>2</sup>*Basic Science Program, Korea University of Science and Technology (UST), Daejeon 34113, Republic of Korea*

The present paper is devoted to comprehensive theoretical studies of exciton-polariton quantum fluids specificities in the optics of their utilization for quantum turbulence research. We show that a non-trivial implementation of time-varying potential for excitation of quantum fluid (injection of quantized vortices) via the stirring procedure can be efficiently substituted with resonant excitation-based phase-imprinting techniques. The most efficient phase pattern corresponds to imprinting of tiles with randomly oriented plane waves in each. The resulting turbulent flows, spatial vortex distributions, and clustering statistics resemble those for the case of a conventional spoon-stirring scheme. We quantify the limitations on the lifetime and density depletion for the development and sustainability of quantum turbulence. The yield is the necessity to prevent the density depletion for more than one order of magnitude. Finally, we demonstrate that turbulence is robust with respect to alternating gain and loss at a certain range of modulation parameters, which corresponds to laser operating above and below condensation threshold.

## I. INTRODUCTION

Quantum turbulence is a peculiar stochastic phenomenon characterized by the emergence of a spontaneous order from chaotic motion, due to the formation of self-similar spatial structures of vorticity topological defects in a quantum fluid. Contrary to the observations of 3D quantum turbulence in quantum systems, such as superfluid helium [1, 2] and ultra-cold atomic Bose-Einstein condensates [3, 4], the existence of an inverse cascade for 2D quantum turbulence analogous to the one observed in classical fluids is still under strong debate, due to both controversial scaling arguments and very stringent mathematical limits on numerical simulations [5]. Indeed, while several works have numerically confirmed the dynamical clustering of quantized vortices, namely the Onsager vortex clustering, consistently with the inverse energy cascade by means of evaporating heating process [6–9], other argue against its existence [10]. Today, thanks to recent technological advancements in spectroscopy and semiconductor manufacturing, polariton quantum fluids, with their hybrid light-matter nature, represent an alternative platform for investigating 2D quantum turbulence [11].

The exciton-polariton is a bosonic composite quasi-particle, formed in semiconductor microcavities by the exciton (electron-hole hydrogen-atom-like quasiparticle) strongly coupled to the cavity photon, and undergoes a strong radiative decay because of the finite lifetime of its photonic component. Compared to the long-living atomic systems, this essential feature, in addition to the very small effective mass of polariton, distinguishes the observed superfluid behavior [12, 13] and Bose-Einstein condensation [14] in polaritonic systems. The latter exhibit a high critical temperature (very small effective mass) and a driven-dissipative nature, which experimentally can be overcome by means of external optical incoherent pumping [15]. The dynamics of topological defects has been extensively investigated. The the experi-

mentally estimated healing length value  $\xi$  (order of a micrometer) of quantized vortices [16–18] allows, in principle, the chance to observe an inverse energy cascade over a larger range of magnitude of the wave vector (upper cascade bound  $1/\xi$ ). Moreover, the quantized vortex creation method (in other words, the energy injection method) plays a crucial role in the observation of the energy cascade both theoretically and experimentally, and techniques such as spoon-stirring [19, 20], paddle or defect grid drag [21, 22] of fluid flowing around stationary defects [23] have been used in the past as a standard vortex injection technique for atomic systems.

The necessity to implement a time-varying potential challenges the implementation of conventional spoon-stirring quantized vortex injection scheme for exciton polariton systems. Currently, among the setups based on the time-varying potential for polariton quantum fluid excitation, one should highlight the single-vortex creation in the rotating-bucket experiments [24–26]. However, polaritons are suitable for direct wave function imprinting via the quasi-resonant excitation approach with flexible spatial light modulator-based (SLM) phase engineering. This approach was successfully used to excite complex spatial distributions of quantized vortices [27, 28]. It is necessary to find reliable approaches for that type of excitation that are able to reproduce the specificity of conventional spoon stirring in the framework of vortex clustering and spectral energy distribution. In this study, we propose various wave function phase patterns and show that those of tiles of plane waves with randomly directed wave vectors effectively mimic the spoon-stirring method of vortex injection.

Next, the important specificity of polaritons is finite lifetime. Previously, the effects of the finite lifetime of polaritons were investigated in Ref. [29] with the main emphasis on tracking the time dynamics of vortex spacing, dipole moments and vorticity correlation function. It remains important to study incompressible kinetic energy spectra during the decay process, and this study

covers this gap.

Finally, we investigate the effects of gain/loss fluctuations on the reliable existence of quantum turbulence. First, we impose experimental limitations on the required stability of laser power to maintain the turbulence by the means of incoherent excitation scheme. At the same time, we show that alternating periods of positive and negative gain under certain conditions do not affect the development of the turbulence. Thus, an experimental scheme of the laser periodically operating above and below the condensation threshold can be useful for quantum turbulence experiments: the positive gain phase overcomes the losses, and the negative gain phase provides the unperturbed wave function evolution.

The paper is organized as follows. In section II, we describe in details the scheme of the provided numerical simulation of dissipative quantum fluid dynamics within the framework of Gross-Pitaevskii equation. In subsection III A, the equivalence between imprinting techniques and spoon stirring for quantum turbulence studies is extensively discussed within the framework of spatial distributions, vortex statistics and incompressible kinetic energy (IKE) spectra analysis. Subsection III B focuses on the effects of losses on sustainability of quantum turbulence arising from the finite lifetime specificity of polaritons, studying at which extent quantum fluids density depletion effects on IKE spectra and vortex statistics for quantum fluid with losses. Then, in subsection III C, we investigate the conditions on the existence of reliable quantum turbulence signs in presence of gain/loss fluctuations, modeling the experimental case of a laser operating above and below condensation threshold. The final conclusions and observation are collected in section IV.

## II. NUMERICAL SETUP

In the quantum fluids research field, the widely used theoretical model is the mean-field Gross-Pitaevskii equation-based approach, which efficiently describes a Bose-Einstein condensate in equilibrium. Regarding exciton-polaritons, quasiparticles of finite lifetime, such model represents an idealized conservative description and requires modification by adding the specific terms responsible for the gain and loss:

$$i\hbar \frac{\partial}{\partial t} \psi(\mathbf{r}, t) = (i\beta(t) - 1) \frac{\hbar^2 \nabla^2}{2m} \psi(\mathbf{r}, t) + g|\psi(\mathbf{r}, t)|^2 \psi(\mathbf{r}, t) + V(\mathbf{r}, t) \psi(\mathbf{r}, t) - i \frac{\hbar}{2} \gamma(t) \psi(\mathbf{r}, t). \quad (1)$$

The values for a polariton systems are taken as follows:  $m = 5 \times 10^{-5} m_0$  (bare electron mass  $m_0 = 9.1 \times 10^{-28}$  g),  $g = 5 \times 10^{-3}$  meV $\mu\text{m}^2$ . Eq.(1) is solved by means of third order Adam-Bashforth method for the time integration, with time step  $\Delta t = 0.004$  ps, total duration  $T_{tot} = 4.56$  ns and a square mesh grid of size  $L = 512 \mu\text{m}$ . For the calculation of the Laplace operator, we used

Table I. The quantum fluids densities  $\langle |\psi|^2 \rangle$  in the end of analysis phase with respect to initial one used for simulation and corresponding values of lifetime.

$\frac{\langle  \psi ^2 \rangle(t=T_{tot})}{\langle  \psi ^2 \rangle(t=T_{tot}/2)}$	0.3	0.1	0.03	0.1	$\approx 1$
$\tau$ , ns	1.89	0.99	0.65	0.5	300

the Fourier transform with massive parallelization provide by GPU. The additional  $\beta$ -dependent term comes from the Hybrid Boltzmann Gross-Pitaevskii theoretical model [30], where  $\beta$  parameter governs dissipation related to high wave vectors. The value of  $\beta$  parameter is predicted to be controlled by the temperature from nearly zero value to that comparable to 0.1. For each simulation, we perform averaging over 16 runs.

In this study, we present and validate two different initial configurations of the condensate wave function  $\psi_0 = \psi(\mathbf{r}, t = 0)$  and check their validity by comparison with the classical rotating spoon technique. In both cases, we keep the wave function density constant at the level of **XXX** which gives healing length  $\langle \xi(t) \rangle = \hbar \sqrt{2m \langle |\psi(t)|^2 \rangle} \approx \text{XXX} \mu\text{m}$  and engineer the phase exclusively. In the first case, we divide the wave function into the square tiles of the size  $64 \mu\text{m}$  and fill each of them by randomly oriented plane wave with wave length  $8 \mu\text{m}$  (Tile-8) or  $4 \mu\text{m}$  (Tile-4). In the second case, we divide wave function into pixels of the size  $8 \mu\text{m}$  (Pixel-8) or  $4 \mu\text{m}$  (Pixel-4) of the random phase each. Experimentally, this approach can be straightforwardly implemented based on the quasi-resonant pumping and spatial light modulator usage. Total simulation time was  $T_{tot} = 4.56$  ns. During the first (preparatory) part of the simulation (from 0 to  $T_{tot}/2 = 2.28$  ps), polariton lifetime was set sufficiently higher then simulation duration and decay parameter  $\beta$  was set to **XXXX** allowing the initial phase pattern evolve to the turbulent state. During the second (analysis) part of the simulation from  $T_{tot}/2$  to  $T_{tot}$ , the data for the analysis was collected. For spoon-stirring and tile-imprinting turbulence generation schemes, the density in the beginning of analysis phase was around  $120 \mu\text{m}^{-2}$ , while for pixel schemes one obtains around  $160 \mu\text{m}^{-2}$ . The confining potential of  $480 \mu\text{m}$  in diameter was used. The parameter  $\beta$  was switched to zero and lifetime  $\gamma^{-1}$  was set depending on the required decay rate. We use the values of polariton lifetime listed in Table I, which yield the final density 30%, 10%, 3% and 1% of the initial one (for the analysis phase). These values exceed sufficiently the achievable in actual samples, however they allow establishing fundamental limitations for the polariton platform utilization for quantum turbulence studies. The duration of the spoon-stirring numerical experiment was similar, with stirring phase during the first part and analysis during the second part. More simulation details are given in supplemental materials.

For the analysis, we perform vortex detection and implement clustering algorithm described in section VI of Ref. [7]. It allows calculating the number of free and clustered vortices and of vortex dipoles in each time moment. Knowing the positions of vortices (and chemical potential  $\mu = gn$ ) allows *semi-analytical* calculation of IKE spectra both for full vortex distributions and for clustered vortices only, giving priority to hierarchal structures specific to the turbulence with respect to single vortices and dipoles [31]. The function  $E^{(i)}(k)$  representing the IKE spectrum we are interested in can be calculated as

$$E^{(i)}(k) = N_{vort} \Omega \xi^3 F(k\xi) G(k), \quad (2)$$

where

$$F(k\xi) = \frac{k\xi}{4\Lambda} \left( I_1 \left( \frac{k\xi}{2\Lambda} \right) K_0 \left( \frac{k\xi}{2\Lambda} \right) - I_0 \left( \frac{k\xi}{2\Lambda} \right) K_1 \left( \frac{k\xi}{2\Lambda} \right) \right), \quad (3)$$

and vortex positions and signs define

$$G(k) = 1 + \frac{2}{N_{vort}} \sum_{i=1}^{N_{vort}-1} \sum_{j=i+1}^{N_{vort}} \kappa_i \kappa_j J_0(k|\mathbf{r}_i - \mathbf{r}_j|) \quad (4)$$

with enstrophy quantum  $\Omega = 2\pi\hbar^2 n / (m\xi^2)$ , parameter  $\Lambda = 0.8249$ .

We also perform calculating the IKE spectra fully *numerically*. First, the density weighted velocity field  $u(\mathbf{r}) = -i\hbar / (2m|\psi(\mathbf{r})|) \cdot (\psi^*(\mathbf{r})\nabla\psi(\mathbf{r}) - \psi(\mathbf{r})\nabla\psi^*(\mathbf{r}))$  is calculated and plugged into equation for finding the incompressible ( $i$ ) part:

$$u_\alpha^{(i)}(\mathbf{k}) = \sum_{\beta=x,y} (\delta_{\alpha,\beta} - k_\alpha k_\beta / k^2) u_\beta(\mathbf{k}), \text{ for } \alpha = x, y. \quad (5)$$

The latter, is then used to calculate the IKE spectrum via

$$E^{(i)}(k) = \frac{m}{2} \int d\mathbf{k} \left( |u_x^{(i)}(\mathbf{k})|^2 + |u_y^{(i)}(\mathbf{k})|^2 \right). \quad (6)$$

Furthermore, by means of Eq. (1) with time-dependent loss rate  $\gamma(t)$ , we present a model with sign-alternating polariton gain and loss, which approximates the behavior of the driven-dissipative Gross-Pitaevskii equation (ddGPE) for polariton condensate incoherently pumped by the unstable or intentionally modulated laser operating above and below the threshold. For this set of simulations, we do not employ the confining potential.

### III. RESULTS AND DISCUSSIONS

#### A. Comparison of imprinting techniques and spoon-stirring vortex injection

The main goal of present subsection is to clarify if imprinting techniques are equivalent to spoon stirring for quantum turbulence studies. Therefore, we consider the

data at the very initial time moments of the analysis phase, i.e. from  $T_{tot}/2 = 2.28$  ps to 2.38 ps and average over 10 time moments. We use the resulting wave functions and compare vortex and cluster statistics and IKE spectra for reference spoon stirring procedure of turbulent motion excitation and for that relying on imprinting techniques.

Fig. 1 illustrates the basic principles of the investigated vortex injection and quantum fluid excitation methods. The panels show various stages of the development of turbulence for the spoon stirring procedure and for the imprinting techniques. The obtained for the spoon-stirring procedure density and phase motifs are typical for that kind of vortex injection method, see panels a) and b). For the imprinting technique Tile-8, we plot (panel c) initial phase pattern, that can be sent to SLM device for quasi-resonant polariton excitation. In panel d), we also plot vorticity map at the very beginning (11 ps) of the free evolution. One sees emergence of vorticity singularities at the tile borders that will further develop into distribution of stable quantized vortices. Finally, in panels e) and f) we plot initial phase pattern for Pixel-8 imprinting technique and the density plot for the well-developed turbulence, respectively. One sees that the phase imprinting techniques are capable of creating the turbulent-like state of quantum fluid. The stochastically created vortex seeds (points with non-zero circulation around) then develop into the well-shaped quantized vortices. The videos of the simulations can be found online, see Supplemental for more details.

Fig. 2 shows the results of vortex detection and the application of the clustering algorithm for the cases of the Tile-8 phase-imprinting technique and for the spoon-stirring procedure at the beginning of the analysis phase (for conservative simulation). Visually, the resulting vortex distributions and their organization into clusters nearly coincide for Tile-8 and spoon-stirring. However, a detailed quantitative analysis of the excitation strategies is necessary from the point of view of cluster statistics and IKE spectra.

To do so, we plot histograms to highlight vortex clusterization for all excitation strategies employed. The left counterparts of the paired columns in panel a) in Fig. 3 show the number of single vortices, vortices in dipoles and vortices in clusters at the beginning of the analysis stage for all excitation techniques employed. One can see that Tile-8 strategy resembles the spoon-stirring one much better than other strategies. Fractions of vortices in single state, dipoles and clusters are sufficiently similar. For Tile-4 and Pixel strategies, one observes substantially lower fraction of vortices in clusters. Panel b) in Fig. 3 gives more details on clusterization for spoon stirring and phase imprinting Tile-8 strategy. Tile-8 gives a slightly higher number of vortices in large clusters whereas the spoon-stirring strategy produces more single vortices, dipoles and small clusters. Typical inter-vortex distance  $l$  can be estimated as  $L/\sqrt{N}$ , which gives  $l \approx 20 \mu\text{m}$  for Tile-8 and spoons-stirring strategies.



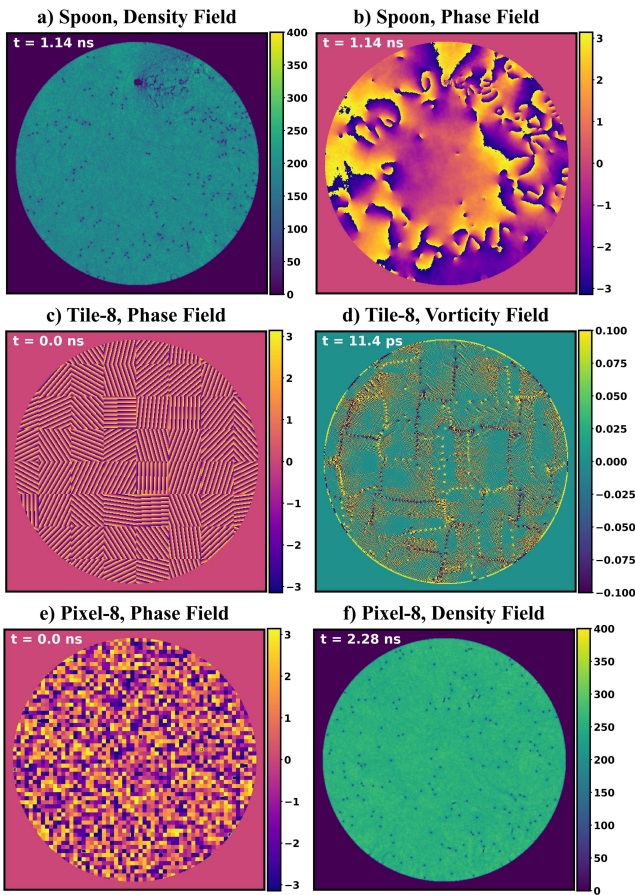


Figure 1. Snapshots of density, phase and vorticity field illustrating various employed quantum fluid excitation schemes. Panels **a)** and **b)** show the density and phase fields, respectively, in the middle of the spoon rotation phase. The typical patterns for such excitation method are visible. The representative initial wave function phase profile for the phase-imprinting strategy Tile-8 (wavelength  $\lambda = 8 \mu\text{m}$ , tile size  $32 \mu\text{m}$ ) is given in panel **c)**, and its evolution after 11.3 picoseconds with multiple vortices appeared at the former tile borders visible as vorticity singularities is given in panel **d)**. The proposed phase pattern can be used for sending to SLM device in experiments. The initial phase pattern for pixel-imprinting (pixel size  $l = 8 \mu\text{m}$ , Pixel-8) is shown in panel **e)**, and the density field in panel **f)** corresponds to the well developed turbulence.

IKE spectra calculated via positions of all vortices and via positions of clustered vortices only (employing Eq. (2)) are depicted in panel a) of Fig. 4 for all excitation strategies. One can see very similar full IKE spectra regardless the strategy employed; the discrepancies are within the values imposed by the difference in the total number of vortices, see Fig. 3. The full IKE spectra are composed of two parts different in characteristic power law. Exponent  $-3$  describes the vortex cores at high wave vectors (greater than  $\xi^{-1}$ ) and exponent  $-1$  dominates at lower wave vectors, being a fin-

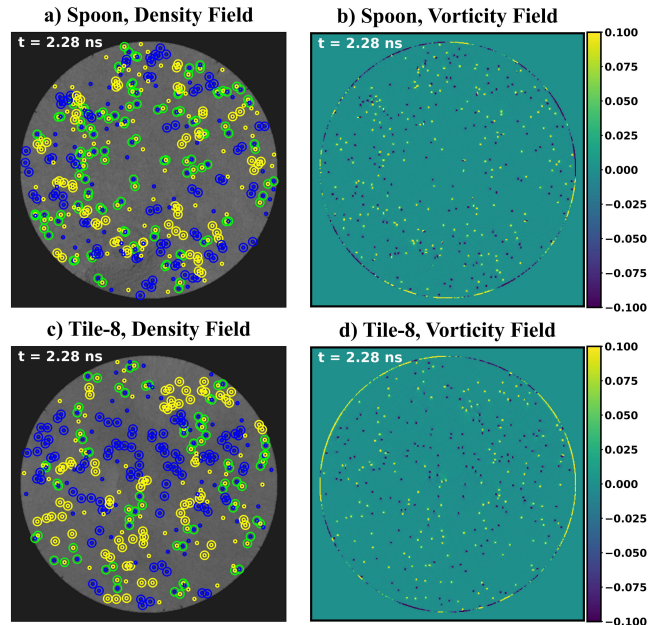


Figure 2. Results of vortex detection followed by clustering algorithm for spoon-stirring (**a,b**) and Tile-8 (**c,d**) excitation. The vortices of opposite signs are denoted with yellow and blue inner circles in density field images (panels **a** and **c**). Vortices belonging to the clusters carry outer circles of the corresponding colors. Green outer circles show the dipoles. Vorticity field is shown in panels **b**) and **d**).

gerprint of an uncorrelated gas of vortices with dominating dipoles and single vortices. At the same time, the spectra for clustered vortices demonstrate a visible region of  $-5/3$  power law, as was shown earlier for different excitation strategies [31]. It should be noted that the Tile-8 phase-imprinting excitation strategy demonstrates full and clustered vortex-based IKE spectra very similar to those of the spoon-stirring approach. Among the phase-imprinting techniques, Tile-8 yields the highest clusterization degree comparable to the spoon stirring case. For pixel-type imprinting contribution from clustered vortices is lower, which agrees with the histograms. Panels **b)** and **c)** in Fig. 4 show full IKE spectra obtained semi-analytically via Eq. (2) (for full IKE spectra and IKE spectra of clustered vortices) and numerically via Eq. (6) for Tile-8 and spoon stirring cases, respectively. One sees that at low wave vectors (large size scales) full and clustered vortex IKE spectra coincide. This is due to the vanishing global rotational motion from the uncorrelated part of the “vortex gas”. For the wave vectors above  $l^{-1}$ , one sees that full IKE spectra have higher magnitude than the clustered vortex IKE spectra proportionally to the fraction of clustered vortices.

The main conclusion of present section is that the phase-imprinting excitation strategy Tile-8 gives vortex statistics and IKE spectra very close to those of the conventional spoon stirring excitation strategy. Thus,

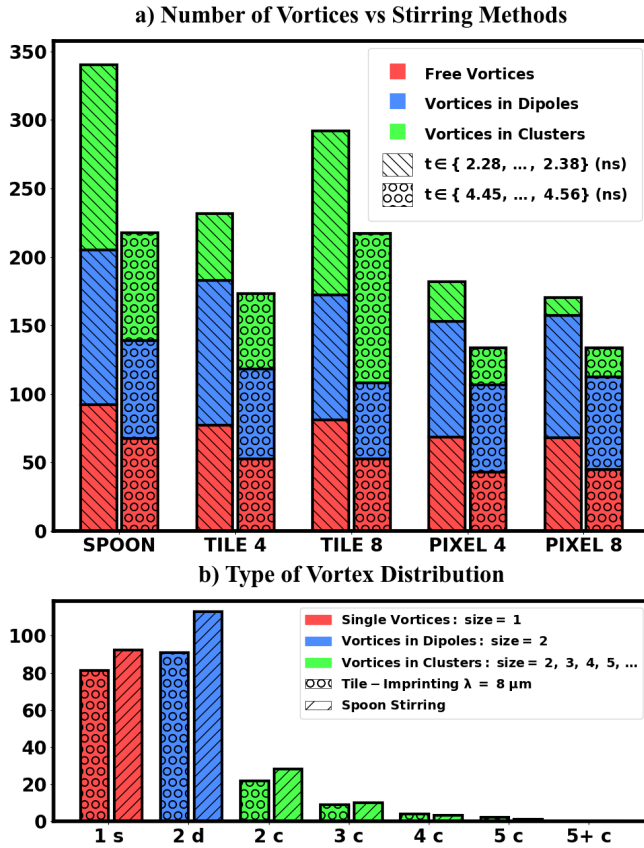


Figure 3. Histograms for vortex statistics results obtained for all excitation strategies. Panel **a)** shows single vortices (red bar parts), vortices in dipoles (blue) and clustered vortices (green) in the beginning of the analysis (left of paired bars) and after 2.38 ns for  $\tau = 1.89$  ns (right of paired bars). Panel **b)** focuses on Tile-8 phase imprinting strategy and spoon-stirring strategy giving details on the number of vortices belonging to clusters of various sizes.

it could be used as a phase pattern sent to SLM for quasi-resonant polariton excitation in experiments. The proposed Tile approaches provide sufficient degree of stochasticity due to random orientations of the flow directions within different tiles. Therefore, one will be able doing both reproducible (for at least initial evolution stages) runs for a phase given pattern for emission signal accumulation and perform averaging over numerous random initial phase patterns.

## B. Effects of losses on sustainability of quantum turbulence

In present section, we investigate at which extent quantum fluid density depletion effects on IKE spectra and vortex statistics of quantum fluid with losses (radiative losses in case of polaritons). At this stage of the analysis, it has been clear that Tile-8 imprinting is valid quantum

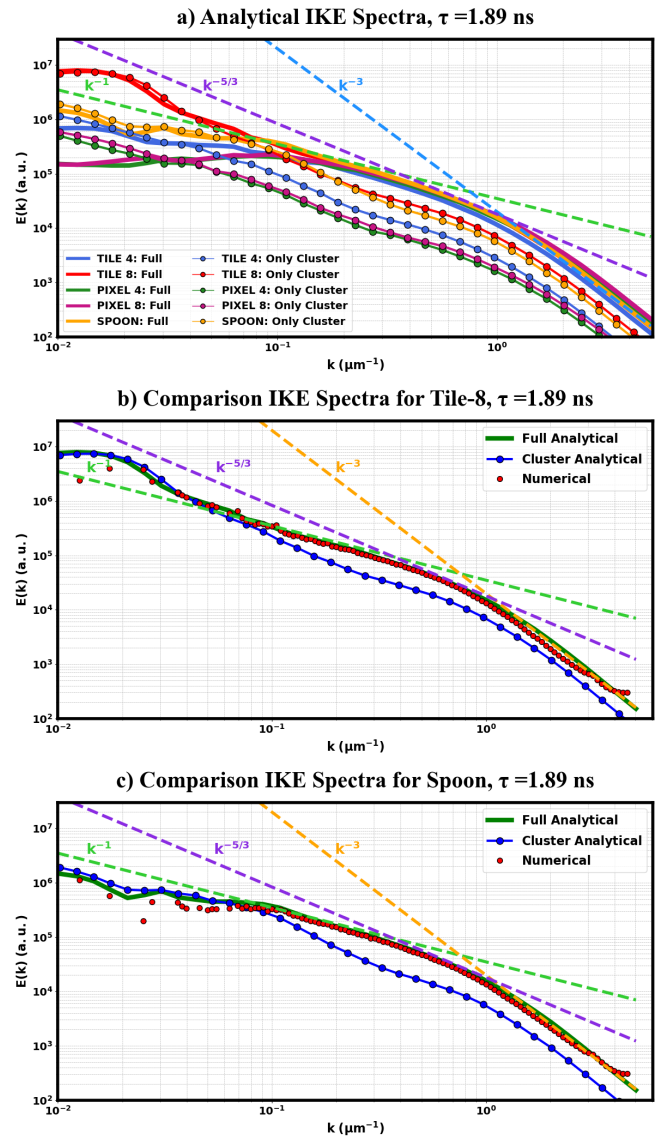


Figure 4. Panel **a)** Results of the Incompressible Kinetic Energy (IKE) spectra semi-analytical calculation (Eq. (2)) for all excitation strategies. Solid curves are for full vortex distributions and curve with dots is for clustered vortices only. Guides for eye are given for characteristic exponents:  $-3$  (vortex core),  $-1$  (dipole),  $-5/3$  (clustered vortices). Panels **b)** presents the comparison of full IKE spectra obtained semi-analytically and numerically and IKE spectra obtained semi-analytically for clustered vortices for Tile-8 excitation. Panel **c)** is the same for the spoon-stirring approach.

fluids excitation method to study quantum turbulence, as shown by the analysis of the IKE spectra and vortex statistics. So, we focus on this excitation method. First, we track the time evolution of quantum fluid density and total number of vortices, see Fig. 5 panels a) and b), respectively. One sees that for high lifetime the decay of the total number of vortices is very close to the conservative case. For stronger decay, decrease of total number

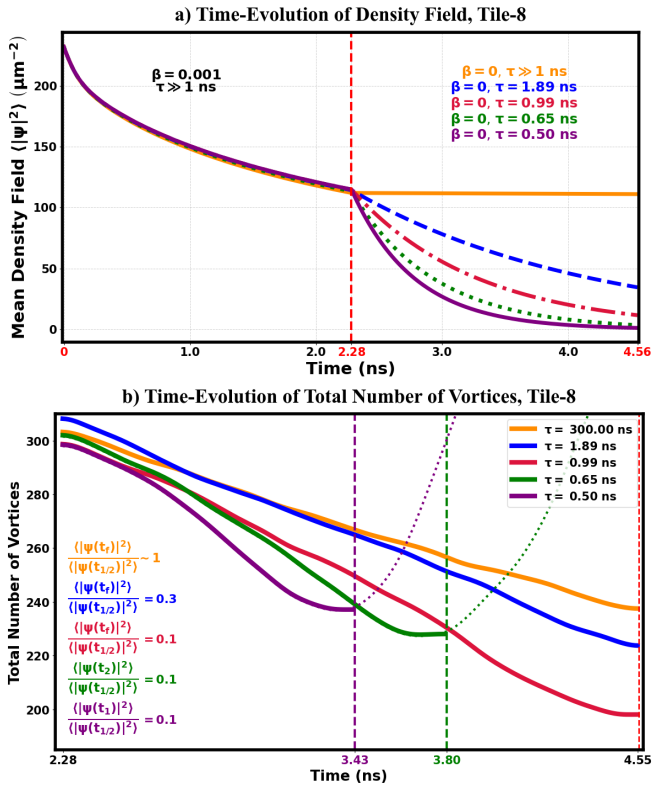


Figure 5. Time evolution of quantum fluid density (a) and total number of vortices (b) for various values of quantum fluid lifetime  $\tau$  for Tile-8 excitation.

of vortices is stronger. When the density reaches approximately  $20 \mu\text{m}^{-2}$  (or 10% of density in the beginning of analysis phase), an abrupt raise in number of vortices in the automatized detection procedure becomes visible, which corresponds to turbulence vanishment associated with appearance of the noise-like phase pattern. However, for lifetimes higher than 1 ps, turbulence exists for the whole observation period.

Fig. 6 shows separation of the whole vortex ensemble into single vortices, dipoles and clusters for  $\tau = 1.89$  ns and  $\tau = 0.99$  ns compared to the conservative case. One can see that the lifetime for the typical polariton parameters (effective mass and interaction constant) giving the vortex evaporation dynamics as in the conservative case should be higher than 1 ns. Direct comparison of the vortex statistics after 2.38 ns of evolution with the initial one is given above in Fig. 3. It is worth mentioning that the chosen parameters except lifetimes are typical for the exciton-polaritons in semiconductor microstructures and therefore the conclusions regarding the required lifetimes are quite general for the exciton-polariton systems.

It is also important to analyze the IKE spectra during the quantum fluid decay process. Fig. 7 shows the semi-analytical IKE spectra of the quantum fluid with finite lifetime  $\tau = 1.89$  ns at various time moments. One can see the smooth evolution of spectra with time visible in

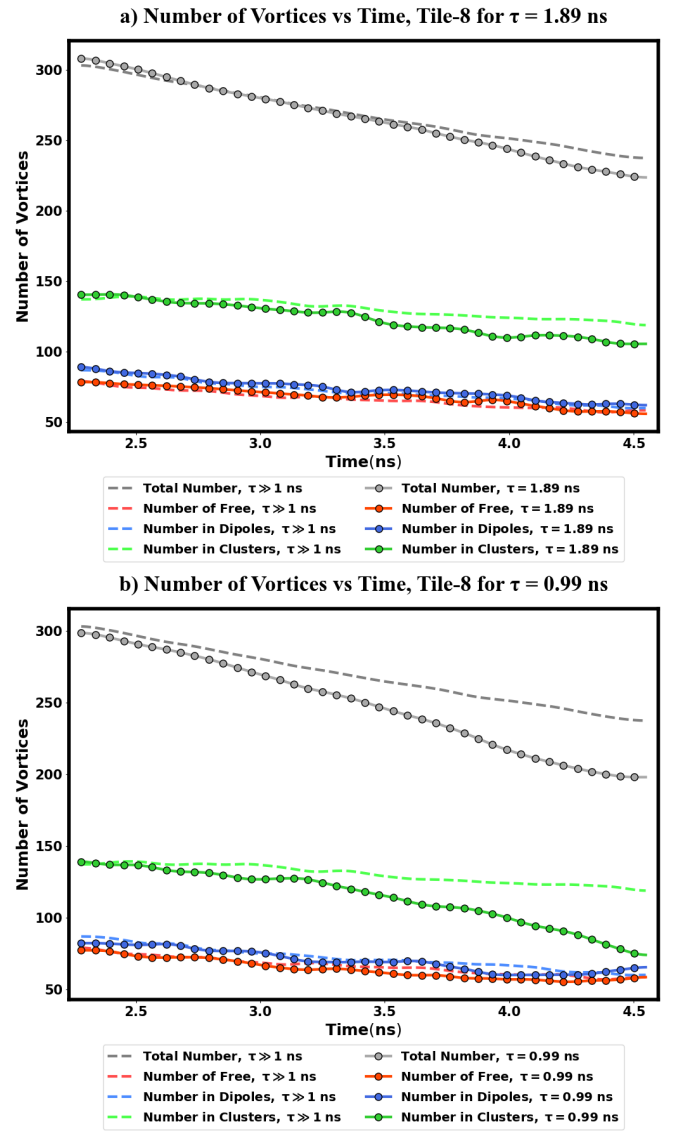


Figure 6. Time evolution of the number of single vortices (red color), vortices in dipoles (blue) and in clusters (green) for lifetimes  $\tau = 1.89$  ns (panel a) and for lifetime  $\tau = 0.99$  ns (panel b). Gray color is for total amount of vortices. Dashed curves give the results for the conservative case.

overall lowering of incompressible kinetic energy at all time scales. At the same time, decay at wave vectors of the order of  $\xi^{-1}$  and higher is stronger than that at low wave vectors, which is a fingerprint of the conservation of the global rotational motion.

Moreover, we are interested in further analyzing (using the tile-imprinting scheme) formation of clouds of vortices with the same sign as polariton decay, which can be quantified via the nearest-neighbor sign correlation function  $C$  as in Ref. [28]. In fact, non-zero positive values of the function  $C$  highlight the emergence of a spontaneous order from chaotic motion, resulting in a low entropic state (negative vortex temperature) [6, 32, 33]. Fig.



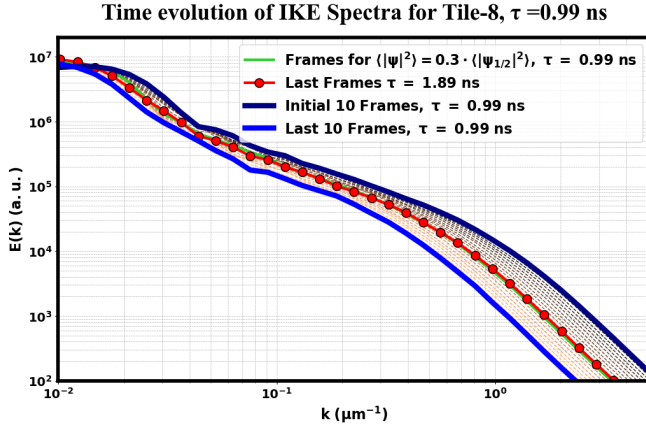


Figure 7. IKE spectra evolution for decaying quantum fluid with lifetime  $\tau = 1.89$  ns. Dark blue curve is for initial IKE spectrum and blue one is for spectrum after 2.38 ns evolution. Dashed lines in blue-green gradient colors show intermediate stages for each XXX ps. Green curve shows spectrum for time moment 3.57 ns where the density is 0.3 of initial density. Red curve is given for comparison with the case of  $\tau = 0.99$  ns for the final stage of simulation with density also of 0.3 of initial one. One can conclude that IKE spectrum depends primarily on the density but not on the decay rate if decay is slow enough.

8 shows, for Tile-8 (panel a) and classical spoon (panel b) strategies, the time evolution of correlation function  $C$  evaluated at the previously considered different quantum fluid loss rates (or equivalently polariton lifetimes). The behavior of the correlation function clearly confirms the existence of clouds of vortices with the same circulation sign for Tile-8 during all the entire simulation duration for  $\tau = 1.89, 0.99$  ns, as well as decaying and vanishing turbulence with a fast transition towards the negative values for lifetime values below 1 ns. Interestingly, that unlike ambiguous results of vortex statistics and IKE spectra analysis, correlation function is capable to distinguish Tile-8 and spoon stirring excitation showing higher organization in the former. One can notice how for Tile-8 excitation strategy more pronounced vortex clustering originates from the formation of “streets of vortices” at tile borders since the very initial evolution stage, see Fig.2(d).

For both Tile-8 and spoon-stirring approaches, one can see the slow growth of  $C$  correlation function corresponding to the evaporative-heating mechanism arising from the vortex annihilation occurring at the border of trap and in vortex dipoles, in agreement with Ref. [29]. From the given analysis, one can conclude that it is necessary to maintain the turbulence for at least several nanoseconds (and thus have the comparable lifetime) to detect the evaporative-heating effect fingerprints. A dissipative phenomenon as the radiative polariton decay significantly compromises this process, because of vortex core expansion slowing down the vortex dynamics, with a con-

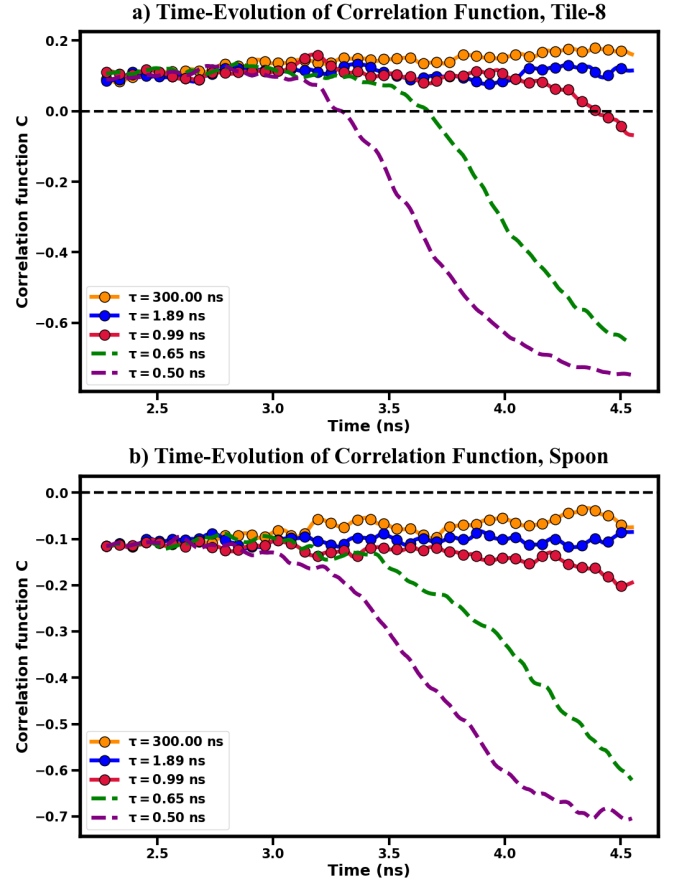


Figure 8. Time evolution of the nearest-neighbor vorticity sign correlation function  $C$  for various lifetimes for Tile-8 imprinting (panel a) and spoon stirring (panel b) strategies. Dashed curves correspond to the noise-like state of the low-density quantum fluid and the turbulence vanished.

sequent conversion of IKE into a compressible energy and emergence of a several random distributed vortex singularities in the system. The important outcome is that for slow decay, IKE spectrum depends on initial configuration and on quantum fluids density, but not on the decay itself.

### C. Quantum turbulence in the regimes of fluctuating gain and loss

In the present section, we investigate the possibility of maintaining quantum turbulence in the regime with alternating phases of positive and negative gain. For polaritons, the regime corresponds to the incoherent pump above and below the threshold. We intend to characterize the effects of gain/loss fluctuations, possibly arising either from intentionally modulated lasers or from experimental limitations on the optical laser stability.

We consider two regimes of gain/loss modulation. For the “cosine” regime, we set  $\gamma(t) = \gamma_0 \cdot \cos(2\pi/T \cdot t)$  in

Eq. 1, where effective  $\gamma_0^{-1} = \tau = 25$  ps, which is close to the values of lifetime in the actual polariton platforms. Practically,  $\gamma(t)$  is defined by the combination of polariton radiative losses and stimulated scattering from the exciton reservoir. The “bar” regime is designed to be more stochastic. It corresponds to a rectangular profile of absolute value  $\gamma_0$  modulated with alternating positive and negative signs with characteristic duration of the order of  $T$ , to be specific taken as a random value from the range  $[0.5 \dots 2.0] \cdot T$ . The insets in Fig. 9 illustrate the employed modulation schemes. To quantify the sustainability of the turbulence, we employ the following procedure. First, we repeat the vortex detection procedure described in the previous subsections. Then we calculate the value  $J(X(T)) = \min(X(T), X_{\text{conserv}}) / \max(X(T), X_{\text{conserv}})$  that can be referred to as the “Jaccard similarity for the values”, where  $X(T)$  stands for the number of all vortices, vortices in clusters and dipoles, and single vortices at the end of the simulation for a given characteristic modulation period  $T$ . For significant difference with conservative case, i.e.  $X(T) \gg X_{\text{conserv}}$  or  $X(T) \ll X_{\text{conserv}}$  one obtains  $J$  values are close to 0. The main panels in Fig. 9 demonstrate  $J$  values for cosine and bar types of gain/loss modulation. One sees that the turbulence remains maintained at  $T/\tau$  of the order of unity, again demonstrating the condition of keeping fluctuations of the quantum fluid density less than one order in magnitude. For cosine modulation, the turbulence is maintained at a higher level  $T$  due to the absence of long loss periods.

This is also visible in Fig.10, which shows the results of vortex detection and the application of the clustering algorithm for the cases of  $T/\tau = 0.6$  at the initial frames of evolution and  $T/\tau = 4.6$  at two frames taken during gain and loss intervals,  $t = 2.8$  ns and  $t = 4.1$  ns, respectively. In the first case turbulent motion is still reliable, due to smaller oscillations of the mean density, around the initial density  $n_0 = |\psi_0|^2 = 200 \mu\text{m}^2$ , differently from the  $T/\tau = 4.6$  cases, in which during the depletion intervals the strong dissipation generates new randomly distributed vortex pairs.

Based on these evidences, one can conclude that the quantum turbulence evolution remains unperturbed only if the time scale of gain/loss modulation is smaller than the magnitude of modulation or at most comparable to it. Thus, potential utility of the polariton platform for quantum turbulence studies can be in the experimental protocol of the laser periodically operating above and below the condensation threshold. The positive gain phase would allow for the overcoming of polariton losses, while the negative gain phase would provide the unperturbed evolution to turbulent motion of the condensate wave function.

## Vortex Statistics vs Time-Oscillation Parameter $T$

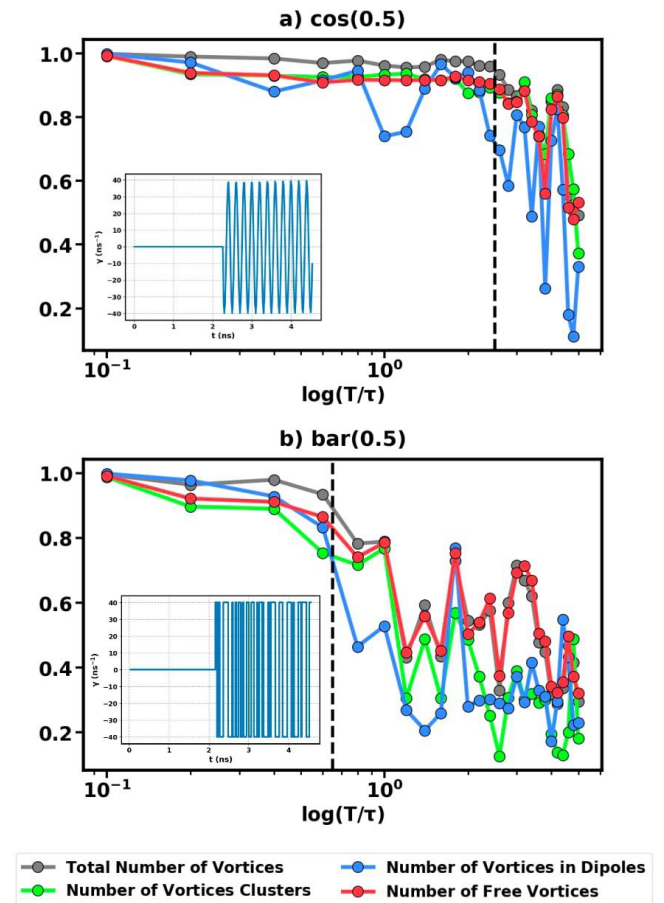


Figure 9. Sustainability of quantum turbulence for the regime of alternating gain/loss with characteristic modulation period  $T$ . The quantity  $J(X(T)) = \min(X(T), X_{\text{conserv}}) / \max(X(T), X_{\text{conserv}})$  is plotted for  $X$  standing for vortex statistical properties: number of all vortices, single vortices, vortices in clusters and dipoles at the end of the simulation. Panel a) is for cosine modulation and panel b) is for bar-shaped modulation. The right side from the vertical dashed lines refers to the regimes where the turbulence is significantly affected by gain/loss modulation. The insets demonstrate typical  $\gamma(t)$  profiles.

## IV. CONCLUSION

In this work, we studied the 2D quantum turbulence with a focus on the inclusion of important specialties inherent to quantum fluids of exciton-polaritons in semiconductor microcavities. The first exciton-polariton feature complication the turbulence studies in a non-trivial implementation of the spoon-stirring vortex injection for turbulence development. However, we demonstrate robustly that one can effectively generate turbulence by direct imprinting the wave function with homogeneous magnitude and phase formed of tiles with randomly oriented plane waves. In experimental implementation of



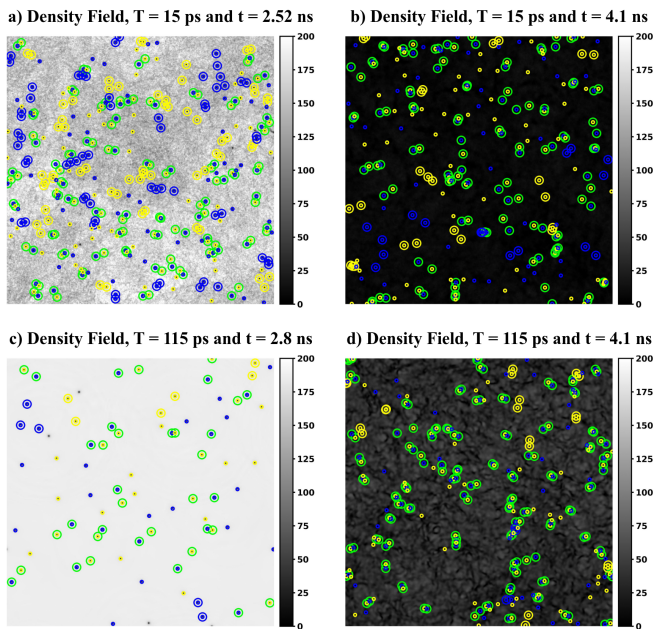


Figure 10. Results of vortex detection followed by clustering algorithm for bar-shaped time modulation with  $T = 15$  ps  $= 0.6 \cdot \tau$  (**a,b**) and  $T = 115$  ps  $= 4.6 \cdot \tau$  (**c,d**). The panels on the left (**a,c**) show snapshot at the beginning of the evolution. Instead, on the right panels (**b,d**) show frames for the dissipation phase.

this scheme, one can use SLM with quasi-resonant laser excitation. The size of the tiles should be comparable to the desired distance between the layers. The created pattern automatically creates phase singularities, which then evolve into quantized vortices. After a certain free evolution period, the resulting statistics of the vortex and incompressible kinetic energy spectra are very similar to those of the conventional spoon-stirring technique. For clustered vortex only, we see the  $-5/3$  exponent in the IKE spectrum that is likely related to Kolmogorov law. The slightly higher clusterization for Tile-8 scheme is visible in the  $C$  correlation function for the signs of nearest neighbors. The randomness of the imprinted wave vector directions in Tile-8 provides the inherent stochasticity of

quantum turbulence and is useful for averaging both for numerical simulations and for experimental realizations. At the same time, the imprinting scheme can allow one to collect the signal in repetitive experiments. Therefore, we conclude that the Tile-8 imprinting scheme is a valid alternative to conventional spoon stirring to study quantum turbulence in quantum fluids. Excitation with pixel random phase is also capable to generate vortices, however, efficiency of generation is significantly lower in this case. Moreover, creation of turbulent-like flows and clusters is also less effective for pixel schemes, which means that the tile schemes possess important features not occurring in more random approach.

Secondly, we show that quantum turbulence can be robust with respect to polariton decay. The statistical quantities like the total number of vortices, the fraction of single and clustered vortices, fraction of vortices belonging to the dipoles evolve smoothly with depletion of the polariton density. The spectral characteristics of the quantum fluid also evolve smoothly. For sufficiently slow decay rate (high lifetimes), IKE spectra do not depend on the decay rate itself, but only on the current density. In general, the fingerprints of turbulence in statistics and IKE spectra remain until approximately one-order decrease of the quantum fluid density. With respect to observation of the evaporative heating effect, one should track the system for at least several nanoseconds for the typical polariton mass and interaction strength, which imposes the respective limitation on the lifetime. Finally, we justify that gain/loss fluctuations do not affect the observation of turbulence under certain conditions on the involved time scales, highlighting the potential utility in quantum turbulence experiments of an experimental scheme of the laser periodically operating above and below the condensation threshold with characteristic period less than polariton lifetime.

## ACKNOWLEDGEMENTS

The authors acknowledge the financial support from the Institute for Basic Science (IBS) in the Republic of Korea through the YSF project IBS-R024-Y3. We thank Oleg I. Utesov for useful remarks.

- 
- [1] W. F. Vinen, Mutual friction in a heat current in liquid helium ii i. experiments on steady heat currents, *Proceedings of the Royal Society of London. Series A. Mathematical and Physical Sciences* **240**, 114 (1957).
  - [2] L. Skrbek, Quantum turbulence, in *Journal of Physics: Conference Series*, Vol. 318 (IOP Publishing, 2011) p. 012004.
  - [3] M. Tsubota, M. Kobayashi, and H. Takeuchi, Quantum hydrodynamics, *Physics Reports* **522**, 191 (2013).
  - [4] A. C. White, B. P. Anderson, and V. S. Bagnato, Vortices and turbulence in trapped atomic condensates, *Proceedings of the National Academy of Sciences* **111**, 4719 (2014).
  - [5] M. Tsubota, K. Fujimoto, and S. Yui, Numerical studies of quantum turbulence, *Journal of Low Temperature Physics* **188**, 119 (2017).
  - [6] T. Simula, M. J. Davis, and K. Helmerson, Emergence of order from turbulence in an isolated planar superfluid, *Physical review letters* **113**, 165302 (2014).
  - [7] R. N. Valani, A. J. Groszek, and T. P. Simula, Einstein-bose condensation of Onsager vortices, *New Journal of Physics* **20**, 053038 (2018).

- [8] T.-L. Horng, C.-H. Hsueh, S.-W. Su, Y.-M. Kao, and S.-C. Gou, Two-dimensional quantum turbulence in a nonuniform Bose-Einstein condensate, *Physical Review A—Atomic, Molecular, and Optical Physics* **80**, 023618 (2009).
- [9] T. Billam, M. Reeves, and A. Bradley, Spectral energy transport in two-dimensional quantum vortex dynamics, *Physical Review A* **91**, 023615 (2015).
- [10] R. Numasato, M. Tsubota, and V. S. L’vov, Direct energy cascade in two-dimensional compressible quantum turbulence, *Physical Review A—Atomic, Molecular, and Optical Physics* **81**, 063630 (2010).
- [11] N. G. Berloff, Turbulence in exciton-polariton condensates, arXiv preprint arXiv:1010.5225 (2010).
- [12] I. Carusotto and C. Ciuti, Probing microcavity polariton superfluidity through resonant rayleigh scattering, *Physical review letters* **93**, 166401 (2004).
- [13] A. Amo, J. Lefrère, S. Pigeon, C. Adrados, C. Ciuti, I. Carusotto, R. Houdré, E. Giacobino, and A. Bramati, Superfluidity of polaritons in semiconductor microcavities, *Nature Physics* **5**, 805 (2009).
- [14] J. Kasprzak, M. Richard, S. Kundermann, A. Baas, P. Jeambrun, J. M. J. Keeling, F. Marchetti, M. Szymańska, R. André, J. Staehli, et al., Bose-Einstein condensation of exciton polaritons, *Nature* **443**, 409 (2006).
- [15] G. Roumpos, M. D. Fraser, A. Löffler, S. Höfling, A. Forchel, and Y. Yamamoto, Single vortex-antivortex pair in an exciton-polariton condensate, *Nature Physics* **7**, 129 (2011).
- [16] K. G. Lagoudakis, M. Wouters, M. Richard, A. Baas, I. Carusotto, R. André, L. S. Dang, and B. Deveaud-Plédran, Quantized vortices in an exciton-polariton condensate, *Nature physics* **4**, 706 (2008).
- [17] L. Dominici, G. Dagvadorj, J. M. Fellows, D. Ballarini, M. De Giorgi, F. M. Marchetti, B. Piccirillo, L. Marrucci, A. Bramati, G. Gigli, et al., Vortex and half-vortex dynamics in a nonlinear spinor quantum fluid, *Science advances* **1**, e1500807 (2015).
- [18] K. G. Lagoudakis, F. Manni, B. Pietka, M. Wouters, T. C. H. Liew, V. Savona, A. V. Kavokin, R. André, and B. Deveaud-Plédran, Probing the dynamics of spontaneous quantum vortices in polariton superfluids, *Physical review letters* **106**, 115301 (2011).
- [19] M. Reeves, B. Anderson, and A. Bradley, Classical and quantum regimes of two-dimensional turbulence in trapped Bose-Einstein condensates, *Physical Review A—Atomic, Molecular, and Optical Physics* **86**, 053621 (2012).
- [20] M. T. Reeves, K. Goddard-Lee, G. Gauthier, O. R. Stockdale, H. Salman, T. Edmonds, X. Yu, A. S. Bradley, M. Baker, H. Rubinsztein-Dunlop, et al., Turbulent relaxation to equilibrium in a two-dimensional quantum vortex gas, *Physical Review X* **12**, 011031 (2022).
- [21] G. Gauthier, M. T. Reeves, X. Yu, A. S. Bradley, M. A. Baker, T. A. Bell, H. Rubinsztein-Dunlop, M. J. Davis, and T. W. Neeley, Giant vortex clusters in a two-dimensional quantum fluid, *Science* **364**, 1264 (2019).
- [22] S. P. Johnstone, A. J. Groszek, P. T. Starkey, C. J. Billington, T. P. Simula, and K. Helmersson, Evolution of large-scale flow from turbulence in a two-dimensional superfluid, *Science* **364**, 1267 (2019).
- [23] M. T. Reeves, T. P. Billam, B. P. Anderson, and A. S. Bradley, Inverse energy cascade in forced two-dimensional quantum turbulence, *Physical review letters* **110**, 104501 (2013).
- [24] Y. del Valle-Inclan Redondo, C. Schneider, S. Klembt, S. Hoofling, S. Tarucha, and M. D. Fraser, Optically driven rotation of exciton-polariton condensates, *Nano Letters* **23**, 4564 (2023).
- [25] I. Gnusov, S. Harrison, S. Alyatkin, K. Sitnik, J. Töpfer, H. Sigurdsson, and P. Lagoudakis, Quantum vortex formation in the “rotating bucket” experiment with polariton condensates, *Science Advances* **9**, eadd1299 (2023).
- [26] I. Gnusov, S. Harrison, S. Alyatkin, K. Sitnik, H. Sigurdsson, and P. G. Lagoudakis, Vortex clusters in a stirred polariton condensate, *Physical Review B* **109**, 104503 (2024).
- [27] T. Boulier, H. Terças, D. Solnyshkov, Q. Glorieux, E. Giacobino, G. Malpuech, and A. Bramati, Vortex chain in a resonantly pumped polariton superfluid, *Scientific reports* **5**, 9230 (2015).
- [28] R. Panico, G. Macorini, L. Dominici, A. Gianfrate, A. Fieramosca, M. De Giorgi, G. Gigli, D. Sanvitto, A. S. Lanotte, and D. Ballarini, Dynamics of a vortex lattice in an expanding polariton quantum fluid, *Physical Review Letters* **127**, 047401 (2021).
- [29] P. Comaron, R. Panico, D. Ballarini, and M. Matuszewski, Dynamics of onsager vortex clustering in decaying turbulent polariton quantum fluids, arXiv preprint arXiv:2402.01637 (2024).
- [30] D. D. Solnyshkov, H. Tercas, K. Dini, and G. Malpuech, Hybrid Boltzmann-Gross-Pitaevskii theory of Bose-einstein condensation and superfluidity in open driven-dissipative systems, *Physical Review A* **89**, 033626 (2014).
- [31] S. Koniakhin, O. Bleu, G. Malpuech, and D. Solnyshkov, 2D quantum turbulence in a polariton quantum fluid, *Chaos, Solitons & Fractals* **132**, 109574 (2020).
- [32] R. H. Kraichnan, Inertial ranges in two-dimensional turbulence, *Physics of fluids* **10**, 1417 (1967).
- [33] A. J. Groszek, M. J. Davis, D. M. Paganin, K. Helmersson, and T. P. Simula, Vortex thermometry for turbulent two-dimensional fluids, *Physical review letters* **120**, 034504 (2018).

## Supplemental Materials

### STIRRING PARAMETERS

We mainly focus on two different physical configurations for the two-dimensional fluid: 1) polaritons with loss rate  $\gamma = 0$ ,  $1/\tau$ , confined by a radially-symmetric hard-bounded potential  $V(\mathbf{r})$ , with diameter  $D = 480 \mu m$ , and stirred by three different methods associated to *stirring potential*  $V_{st}(\mathbf{r}, t)$  and initial state  $\psi_0$ ; 2) unbounded ( $V(\mathbf{r}) = 0$ ) polaritons with loss rate  $\gamma(t)$  oscillating in a time scale defined by the time parameter  $T$ , ( $\gamma(t)$  with cosine-like and bar-like profiles), and stirred by a classical rotating spoon. So, the external potential function  $V(\mathbf{r}, t)$  takes the general form of  $V(\mathbf{r}, t) = V(\mathbf{r}) + V_{st}(\mathbf{r}, t)$ .

The spoon stirring method is performed for a spoon with diameter  $d = 12 \mu m$  and rotating with an orbit of radius  $R_{sp} = 160 \mu m$  and rotation period  $T_0 = T_{tot}/6 = 760 ps$  over a total time interval equal to 3 complete rotation ( $3T_0 = T_{tot}/2$ ). Considering a depth  $V_{max} = 10 meV$ , the associated potential  $V_{st}$  is  $V_{st}(\mathbf{r}, t) = A(t) \cdot H(D/2 - |\mathbf{r} - \mathbf{r}_{sp}(t)|)$ , with  $H$  Heaviside step function and

$$A(t) = V_{max} \cdot \begin{cases} t/T_0 & t \leq T_0 = T_{tot}/6, \\ 1 & T_0 < t \leq 2T_0, \\ (3T_0 - t)/T_0 & 2T_0 < t \leq 3T_0, \\ 0 & t > 3T_0 = T_{tot}/2 \end{cases}, \quad \mathbf{r}_{sp}(t) = L/2 + R_{sp} [\cos(2\pi t/T_0), \sin(2\pi t/T_0)]$$

The time-modulation amplitude function  $A(t)$  is considered to smoothly stir on time the condensate during the whole stirring interval, avoiding to generate excessive density noise. For such a case the initial configuration is  $\psi_0$  is an homogeneous state with density  $n_0 = |\psi_0|^2$ .

While, for the technique proposed as new stirring method, we consider an imprinting of a homogeneous condensate state  $\psi_0$  made of a superposition of plane wavefunctions over a  $8 \times 8$  tile-division of the entire system's grid of size  $L$ , one wavefunction per each tile. The plane waves have the same characteristic wavelength  $\lambda$ , but random directed wavevectors. As the condensate evolves in time, vortices are randomly creates at the borders of the tiles, requiring the presence of no stirring potential ( $V_{st} = 0$ ). With a similar principle, the second technique we propose is imprinting at  $V_{st} = 0$  an homogeneous initial state  $\psi_0$  consisting of a superposition of random-phase wavefunctions in small square pixels of few- $\mu m$  size  $l$ . This two cases, here called *Tile Imprinting* and *Pixel Imprinting*, enables a faster and totally random creation of vortices, few picoseconds, than the stirring by rotating spoon, which takes 2.28 ns to prepare the condensate to the vortex analysis. This is why, in order to obtain comparable vortex configurations for the trapped condensate, for all three stirring cases Eq. (1) is solved for  $\beta = 0.001$ ,  $\gamma = 0$  for  $t \leq T_{tot}/2$  and  $\beta = 0$ ,  $\gamma = 1/\tau$  for  $t > T_{tot}/2$ , but with  $n_0 = 200 \mu m^{-2}$  for the spoon case and  $n_0 = 336 \mu m^{-2}$  for tile and pixel cases, so that  $\langle |\psi|^2 \rangle(t = T_{tot}/2)$  is the same for all cases, and  $\tau = 1.89, 0.99, 0.65, 0.50 ns$ , corresponding to  $\langle |\psi|^2 \rangle(t = T_{tot}) / \langle |\psi|^2 \rangle(t = T_{tot}/2) = 0.3, 0.1, 0.03, 0.01$ .

The solution for time-modulated polariton gain and loss by an oscillating loss rate  $\gamma(t)$ , is carried out for two different time profiles and with  $\beta$  parameter zero during the whole simulation duration. The first corresponds to cosine-like time oscillation described by  $\gamma(t) = 1/\tau \cos(2\pi t/T)$ , with  $T$  the oscillation period. The second profile corresponds to an oscillating function which is a sum of step functions, alternating between  $\pm 1/\tau$ , each defined over a time interval  $T_i = T \cdot rand(0.1, 1)$ . In such a "bar-like" profile, the parameter  $T$  defines maximum the time scale of the decay oscillation. The polariton lifetime is  $\tau = 25 ps$  (typical experimental value), and  $T \in \tau \cdot \{0.1, 0.2, 0.4, \dots, 5\} = \{2.5, 5, 10, \dots, 125\} ps$ . Recalling that the condensate is unbounded and stirred by rotating spoon,  $V(\mathbf{r}, t) = V_{st}(\mathbf{r})$  according to Eq. (IV), we analyze this model considering both  $\gamma(t) \neq 0, \forall t$ , ( $cos(1)$  and  $bar(1)$  cases) and  $\gamma(t) = 0$  for  $t \leq T_{tot}/2$ ,  $\gamma(t) \neq 0$ , for  $t > T_{tot}/2$ , ( $cos(0.5)$  and  $bar(0.5)$  cases).



## LINKS TO THE MOVIES

Here in the present section, we provide a list of links to movies of time evolution of the wave function  $\psi(\mathbf{r}, t)$ , by means of the density field  $|\psi(\mathbf{r}, t)|^2$  and phase field of  $\psi(\mathbf{r}, t) |\psi(\mathbf{r}_c, t)| / \psi(\mathbf{r}_c, t)$  (phase rescaled such that it is zero in the center  $\mathbf{r}_c$ ).

Conservative case of long-living polariton with  $\tau \gg 1$  ns:

- [Spoon-Stirring](#)
- [Tile-4 imprinting scheme](#)
- [Tile-8 imprinting scheme](#)
- [Pixel-4 imprinting scheme](#)
- [Pixel-8 imprinting scheme](#)

Decaying polariton case with  $\tau = 1.89$  ns:

- [Spoon-Stirring](#)
- [Tile-4 imprinting scheme](#)
- [Tile-8 imprinting scheme](#)
- [Pixel-4 imprinting scheme](#)
- [Pixel-8 imprinting scheme](#)